Journal of Engineering for Gas Turbines and Power, Volume 138, Issue 8, August 2016,
Article number 081202; Paper number GTP-15-1539; DOI:10.1115/1.4032652

Aerodynamic Design of Separate-Jet Exhausts for Future Civil Aero-Engines, Part 2: Design Space Exploration, Surrogate Modeling, and Optimization

Ioannis Goulos
Propulsion Engineering Centre
Cranfield University
Bedfordshire, MK430AL, UK
Email: i.goulos@cranfield.ac.uk

John Otter
Propulsion Engineering Centre
Cranfield University
Bedfordshire, MK430AL, UK
Email: j.j.otter@cranfield.ac.uk

Tomasz Stankowski
Propulsion Engineering Centre
Cranfield University
Bedfordshire, MK430AL, UK
Email: t.stankowski@cranfield.ac.uk

David MacManus
Propulsion Engineering Centre
Cranfield University
Bedfordshire, MK430AL, UK
Email: D.G.Macmanus@cranfield.ac.uk

Nicholas Grech
Installation Aerodynamics
Rolls-Royce plc
Trent Hall 2.2, SinA-17, Derby, UK
Email: Nicholas.Grech@Rolls-Royce.com

Christopher Sheaf
Installation Aerodynamics
Rolls-Royce plc
Trent Hall 2.2, SinA-17, Derby, UK
Email: Christopher.Sheaf@Rolls-Royce.com

ABSTRACT

The aerodynamic performance of the bypass exhaust system is key to the success of future civil turbofan engines. This is due to current design trends in civil aviation dictating continuous improvement in propulsive efficiency by reducing specific thrust and increasing bypass ratio. This paper aims to develop an integrated framework targeting the automatic design optimization of separate-jet exhaust systems for future aero-engine architectures. The core method of the proposed approach is based on a standalone exhaust design tool comprising modules for cycle analysis, geometry parameterization, mesh generation, and Reynolds Averaged Navier–Stokes (RANS) flow solution. A comprehensive optimization strategy has been structured comprising Design Space Exploration (DSE), Response Surface Modeling (RSM) algorithms, as well as state-of-the-art global/genetic optimization methods. The overall framework has been deployed to optimize the aerodynamic design of two civil aero-engines with separate-jet exhausts, representative of current and future engine architectures, respectively. A set of optimum exhaust designs have been obtained for each investigated engine and subsequently compared against their reciprocal baselines established using the current industry practice in terms of exhaust design.

The obtained results indicate that the optimization could lead to designs with significant increase in net propulsive force, compared to their respective notional baselines. It is shown that the developed approach is implicitly

able to identify and mitigate undesirable flow-features that may compromise the aerodynamic performance of the exhaust system. The proposed method enables the aerodynamic design of optimum separate-jet exhaust systems for a user-specified engine cycle, using only a limited set of standard nozzle design variables. Furthermore, it enables to quantify, correlate, and understand the aerodynamic behavior of any separate-jet exhaust system for any specified engine architecture. Hence, the overall framework constitutes an enabling technology towards the design of optimally configured exhaust systems, consequently leading to increased overall engine thrust and reduced Specific Fuel Consumption (SFC).

Nomenclature

Roman Symbols

$\dot{m}$	Nozzle mass flow, kg/sec
A	Area, m^2
A_{ratio}	Nozzle exit to charging plane area ratio, $= \frac{A_{CP}}{A_{exit}}$
C_D^{Bypass}	Bypass exhaust nozzle discharge coefficient
C_D^{Core}	Core exhaust nozzle discharge coefficient
$C_V^{Overall}$	Exhaust system overall velocity coefficient
C_D^{Zone3}	Zone 3 vent exhaust nozzle discharge coefficient
F_G, F_N	Gross and net propulsive force, N
h_1	Nozzle charging plane height, m
h_2	Nozzle exit plane height, m
L	Length, m
l_{cr}^{cowl}	Non-dimensional core cowl length, $= \frac{L_{cr}^{cowl}}{R_{fan}}$
l_{z3}^{exit}	Non-dimensional location of zone 3 vent exhaust exit, $= \frac{L_{z3}^{exit}}{L_{cr}^{cowl}}$
M_∞	Mach number (free-stream)
M_{z3}^{exit}	Zone 3 vent exhaust exit Mach number, $= \frac{L_{z3}^{exit}}{L_{cr}^{cowl}}$
N	Range of DOE samples
$N_{eval.}$	Number of evaluations
$N_{Pearson}$	Pearson's product-moment of correlation
P	Pressure, Pa
R	Radius, m
$R(\%)$	Percentage range
R_{CP}^{offset}	Charging plane radial offset relative to the nozzle exit plane, m
R_{curve}	Curvature radius, m
R_{fan}	Fan blade radius, m

T	Temperature, K
y_{bp}^{in}	Bypass duct normalized inner line radius, $= \frac{R_{bp}^{in}}{L_{duct}^{in}}$
y_{bp}^{out}	Bypass duct normalized outer line radius, $= \frac{R_{bp}^{out}}{L_{duct}^{in}}$

Greek Symbols

κ_{CP}^{in}	Inner aeroline curvature radius ratio, $= \frac{R_{curve}^{CP,in}}{h_2}$
κ_{CP}^{out}	Outer aeroline curvature radius ratio, $= \frac{R_{curve}^{CP,out}}{h_2}$
κ_{len}^{in}	Nozzle length ratio, $= \frac{L_{in}^{Nozzle}}{h_2}$
ϕ	Performance metric
$\sigma(\%)$	Percentage standard deviation
θ_{CP}^{out}	Outer aeroline slope at the charging plane, deg
θ_{cp}^{plug}	Core plug after-body angle, deg
θ_{cr}^{cowl}	Core cowl angle, deg
$\theta_{in/out}^{hade}$	Aeroline hade angle at the nozzle inlet plane, deg
θ_{nozzle}^{out}	Nozzle outer line exit angle, deg

Superscripts

$()^{amb}$	Referring to ambient conditions
$()^{Base.}$	Referring to the baseline design
$()^{in/out}$	Referring to the inner or outer nozzle aeroline, respectively
$()^{inlet}$	Referring to inlet conditions
$()^{Opt.}$	Referring to the optimum design
$()^{Overall}$	Referring to the overall exhaust system
$()_{CFD}$	Value obtained from direct CFD simulation
$()_{RSM}$	Value obtained from RSM prediction

Subscripts

$()_0$	Referring to total flow conditions
$()_{bp}$	Referring to the bypass exhaust nozzle
$()_{CP}$	Referring to the nozzle charging plane
$()_{cr}$	Referring to the core exhaust nozzle
$()_{Exit}$	Referring to the nozzle exit plane
$()_{st}$	Referring to static flow conditions
$()_{z3}$	Referring to the zone 3 vent exhaust nozzle

1 Introduction

1.1 Background

Current trends in civil aviation indicate an expected increase of aircraft traffic in the future [1]. As a result, there is a concomitant desire to reduce direct operating costs, fuel burn, as well as gaseous and noise emissions. Epstein [2] noted that in order to conceptualize and implement more fuel-efficient and environmentally friendly turbofan engines, substantial advancements need to be achieved with respect to the employed motor and propulsor design technologies. Considering simple-cycle motors, it is expected that future architectures will employ thermodynamic cycles with increased Turbine Entry Temperature (TET) and Overall Pressure Ratio (OPR) to improve the motor's thermal efficiency [2, 3]. The introduction of novel intercooled and intercooled–recuperated turbofan engine cycles has also been investigated by Kyprianidis *et al.* [4–6].

With respect to propulsor design, it is anticipated that future architectures will employ high By-Pass Ratios ($BPR = \frac{\dot{m}_{bypass}}{\dot{m}_{core}}$) combined with lower Fan Pressure Ratios (FPR) to lower specific thrust and improve propulsive efficiency [7]. Specifically, the employed BPR may be of the order of 15+ for large civil engines at mid-cruise conditions. To put this number into perspective, it is noted that current large turbofan engines are designed for values of BPR closer to 11. However, a rise in BPR also results in higher gross to net propulsive force ratio $\frac{F_G}{F_N}$. This is due to the higher engine mass flow increasing the inlet momentum drag for a given net thrust. Indicatively, it is noted that the ratio $\frac{F_G}{F_N}$ changes from roughly 3 to 4 for increasing the BPR from 11 to 16. Consequently, the net propulsive force F_N and SFC of future engines is expected to be more sensitive to variations in gross propulsive force F_G compared to current designs.

The engine's gross propulsive force F_G is linearly dependent on the aerodynamic performance of the exhaust system. This is determined based on the exhaust's ability to produce thrust that is close to its ideal isentropic value [8–10]. Hence, the economic viability and environmental sustainability of future large turbofan engines will be highly dependent on the exhaust system design. This includes the bypass duct, nozzle, and post-exit components. Therefore, it is imperative that aerodynamic performance of the exhaust system is optimized at a relatively early stage within the overall engine design process.

1.2 Exhaust system performance accounting

Medium to high bypass turbofan engines to date are predominantly equipped with separate-jet exhausts. Figure 1 presents a typical axi-symmetric housing geometry for a notional turbofan engine with separate-jets. The bypass nozzle exit flow is separated from the core flow by the core cowl. The bypass and core streams meet and mix downstream of the core nozzle exit. A protruding core plug is usually employed to reduce the core cowl length required for a given nozzle exit area.

The internal pressure and viscous forces within the bypass walls, core cowl, and core plug can be substantial sources of thrust loss. In some cases, the reduction in F_G due to losses associated with the performance of the exhaust system can be of the order of 1.5–2.0% relative to the case of fully-expanded ideal flow [11]. In terms of performance accounting, the actual duct and nozzle performance is related to that of an ideal nozzle through the definition of the non-dimensional discharge and velocity coefficients, C_D and C_V [12, 13]. C_D and C_V relate the actual nozzle mass flow and thrust, respectively, to that corresponding to one-dimensional (1D) isentropic flow expansion to ambient static pressure [13].

1.3 Design optimization of engine exhaust systems

The advent of Computational Fluid Dynamics (CFD) during the past two decades has rendered it a reliable and useful performance prediction tool for the aerodynamic analysis of exhaust nozzles [14, 15]. This has enabled its use as an efficient evaluation method in the context of design optimization. Several cases can be found in the existing literature where the optimization of gas-turbine exhaust nozzles using CFD has been investigated.

Heath *et al.* [16] performed an aerodynamic shape optimization for an axi-symmetric, dual-stream, plug nozzle employed in a supersonic business jet. Free-Form Deformation (FFD) along with third-order B-splines were employed for the parametric geometry representation. The aerodynamic approach was based on a RANS flow-solver applied to a fully-unstructured grid. The discrete-adjoint method [17, 18] along with grid deformation and adaptation were used to obtain the flow-field gradients with respect to perturbations applied to the parametric nozzle geometry. The flow-field gradient information derived from the discrete-adjoint method was utilized by a local optimization method based on Sequential Quadratic Programming (SQP) [19]. The overall approach was used to minimize the integral of near-field pressure disturbances relative to the free-stream flow. Heath *et al.* [16] noted that their method resulted in a gross thrust gain of the order of 0.2% relative the baseline nozzle design.

Clement *et al.* [20] developed an integrated framework for the design optimization of a bypass duct suitable for a high-bypass ratio turbofan engine with a core mounted gearbox. Their design topology involved the fan Outlet Guide Vanes (OGVs), the downstream bypass duct, as well as the circumferential arrangement of structural components such as struts, fairing, and bifurcations. Second-order splines were used for the parametric definition of the bypass duct geometry. The 3D RANS flow solver HYDRA [21] was used to evaluate the steady-state aerodynamic performance of the overall exhaust system. A hybrid optimization strategy was employed comprising an initial Design of Experiment (DOE) coupled with Response Surface Modeling (RSM) and a global optimizer. The design exploration in Ref. [20] incorporated a random sequence generator approach [22]. Surrogate models (RSMs) were subsequently structured based on the DOE results using interpolation based on Radial Basis Functions (RBF) [23]. A Genetic Algorithm (GA) [24] was employed to minimize the total pressure loss within the bypass duct and therefore optimize the design. Clement *et al.* noted that the optimization process was able to reduce the predicted total pressure loss within the duct by 0.1% relative to a baseline design.

Haderlie and Crossley [25] optimized the aerodynamic performance of an axi-symmetric supersonic inlet by modifying the splitter geometry that separates the core and bypass flows. The employed parametric geometry definition was based on Kulfan's Class-Shape function Transformation (CST) method [26]. The CST approach has been proven to be an efficient and non-restrictive parameterization scheme [27]. It has been shown to be able to reduce the required number of design variables and maintain ample freedom in the available design space [28, 29]. A RANS flow-field solution method applied to a multi-block structured grid was used to evaluate the aerodynamic performance of candidate designs. The optimization strategy initiated with a comprehensive DOE based on the Optimal Latin Hypercube (OLH) technique [30]. An analytical surrogate model was subsequently built from the DOE results using Kriging interpolation [31, 32]. The actual optimization approach initiated with the application of a global GA [24] and finalized with the deployment of the local gradient-based method SQP [19]. Optimizations were carried out for total pressure recovery and peak radial distortion intensity at the

inlet's Aerodynamic Interface Plane (AIP). Haderlie and Crossley noted that their method was able to yield improved splitter designs that satisfied the imposed geometric constraints within an acceptable margin of error.

Qiu *et al.* [33] employed an unsteady, continuous, adjoint-based, acoustic propagation method to optimize the design of a low-noise bypass duct for a civil turbofan engine. An analytical approach was employed based on Hicks-Henne shape functions [34] for the parametric representation of the bypass duct and nozzle geometries. Optimization were carried out using a local gradient-based algorithm driven by the Jacobian information derived from the continuous adjoint method. The objective was to minimize the propagation of tonal noise produced by the engine. Qiu *et al.* noted that their approach was able to reduce the Overall Acoustic Sound Pressure Level (OASPL) at the far-field by 2.78db, relative to a notionally defined baseline engine.

1.4 Scope of present work

In light of the preceding discussion, it can be realized that the aerodynamic efficiency of the exhaust system is key to the success of future large turbofan engines. Therefore, it is imperative that the performance of the bypass duct, nozzle, core afterbody, and plug is catered for at an early stage within the engine preliminary design process. This entails the development of a multidisciplinary approach that can predict and optimize the aerodynamic behavior of an exhaust system for a designated engine cycle. As previously discussed, several authors have tackled the optimization of exhaust nozzles for gas-turbine engines [16, 20, 25, 33]. However, previous references have focused either on the optimization of single-stream plug nozzles, or on the noise produced gas-turbine exhaust systems. A holistic approach for the aerodynamic optimization of separate-jet exhausts including the bypass/core duct, nozzle, and post-exit components for civil aero-engines, has not been reported in the existing literature. Furthermore, the impact of future cycles employing higher values of BPR and lower FPR on exhaust system design and optimization, has not been previously investigated nor reported.

Within the context elaborated above, this work aims to develop an integrated approach targeting the design optimization of separate-jet exhaust systems for future aero-engine architectures. The core of the overall method is based on a standalone tool previously developed by the authors [35] for the parametric design and analysis of separate-jet exhausts. The employed method comprises modules for cycle analysis, geometry parameterization, mesh generation, and Reynolds Averaged Navier–Stokes (RANS) flow solution. Within this work, the existing tool is expanded with the implementation of a comprehensive optimization strategy. The developed framework encompasses numerical algorithms for Design of Experiment (DOE), Response Surface Modeling (RSM), and genetic optimization (GA).

The developed methodology has been deployed to optimize the aerodynamic performance of two civil aero-engines with separate-jet exhausts, representative of current and future large turbofan architectures, respectively. Optimum exhaust designs have been obtained for each investigated engine. A comparative evaluation has been carried out between the optimums solutions to assess the impact of future cycles on exhaust system design. The proposed method can be viewed as an enabling technology for the aerodynamic optimization of separate-jet exhaust systems during the stage of preliminary engine design.

2 Numerical approach

2.1 Aerodynamic design of separate-jet exhausts

This work adapts an integrated tool previously developed by the authors [35] for the aerodynamic design and analysis of separate-jet exhaust systems. The developed tool has been named GEMINI (**G**eometric **E**ngine **M**odeler **I**ncluding **N**ozzle **I**nstallation). GEMINI encompasses a generic design approach applicable to a wide-range of civil aero-engines. It is able to design a complete engine exhaust system for a designated engine cycle along with a prescribed set of key engine hard-points. Figure 2 presents an upper-level illustration of the implemented software architecture. The overall method comprises a series of fundamental modeling methods applicable to; engine performance simulation [36], exhaust duct and nozzle aeroline parameterization [29, 37, 38], and viscous-compressible flow solution [39, 40]. A detailed description of each individual numerical modules has been provided in Ref. [35]. Therefore, only a brief-overview of the overall system will be provided in this paper.

A designated set of thermodynamic cycle and geometric design parameters is initially defined. The computational method initiates by analyzing the engine cycle at Design Point (DP) and Off-Design (OD) conditions. Engine performance simulation is carried out for a user-specified number of operating points within the operational envelope. The cycle analysis is carried out using the zero-dimensional (0D) aero-thermal approach (Turbomatch) described by Macmillan [36]. This process essentially sizes the bypass and core exhaust nozzles in terms of flow capacity requirements. Furthermore, it provides a first-order indication of the averaged aero-thermal flow properties at the inlet and exit stations of the bypass and core exhaust ducts and nozzles (Fig. 1). Turbomatch has been previously deployed in several studies available in the existing literature for the prediction of DP, OD, and transient performance of gas turbine engines [41, 42]. For the scope of the present work, the engine is assumed to be operating exclusively at steady-state conditions.

Having established the required flow-capacities, an inverse design approach is employed to obtain a 2D axi-symmetric representation of the bypass and core exhaust aerolines. An example of the 2D axi-symmetric engine geometry produced by GEMINI is shown in Fig. 1. GEMINI has been computationally coupled with an automatic mesh generation tool [39] applicable to 2D axi-symmetric engine geometries with separate-jet exhausts. Thus, among others, GEMINI automatically establishes the computational domain upon which the viscous compressible flow-field can be resolved using a commercial solver [40]. After obtaining a converged CFD solution, the numerical results are automatically post-processed. This procedure determines the bypass and core nozzle discharge coefficients, C_D^{Bypass} and C_D^{Core}, respectively, as well as the overall exhaust system velocity coefficient $C_V^{Overall}$.

2.2 Exhaust system parametric geometry definition

GEMINI incorporates an analytical approach developed by the authors [35] for the parametric geometry definition of separate-jet exhaust systems based on Kulfan's CST functions [29, 37]. The developed method inherits the intuitiveness of Qin's CST variation [38] and extends its applicability to the parametric representation of exhaust ducts and nozzles. Through the developed formulation, the bypass/core duct, nacelle exhaust, and afterbody aerolines have been reduced to a set of analytical expressions. These have been derived as sole functions of a set of standard design parameters such as; nozzle

Charging Plane (CP) to exit area ratio $A_{ratio} = \frac{A_{CP}}{A_{exit}}$, nozzle length ratio $k_{len} = \frac{L_{nozzle}}{h_2}$, aeroline curvature and slope at the nozzle CP location, $R_{curve}^{in/out}$ and θ_{CP}^{out}, respectively, as well as nozzle outlet angles $\theta_{in/out}^{nozzle}$.

In terms of nozzle design, the developed method initializes at the nozzle exit plane using as input the known geometric throat area required for a given flow capacity. The nozzle throat is located at the exit plane for a convergent nozzle. For convergent-divergent nozzles (con-di) an effective con-di ratio is defined, therefore moving the nozzle throat slightly upstream relative to the exit plane. Application of the rolling-ball area estimation method [43] to the nozzle exit plane and upstream CP, results in a series of control points that satisfy the prescribed design parameters. The design of the upstream duct is carried out through direct control of a series of control-points. The user is able to specify the position, aeroline slope, and curvature radius for any set of control-points that he/she wishes to specify along the upstream duct. A mathematical description of the employed geometric parameterization approach has been provided in Ref. [35].

Figure 3 presents a preliminary method application on the design of a 2D axi-symmetric engine exhaust system. It can be observed that the employed parametric geometry includes the design of the engine intake. This is in order to account for the effect of inlet mass flow capture ratio on the aerodynamic behavior of the nacelle exhaust. Accounting for this effect is required to capture the static pressure distribution on the nacelle after-body, and consequently, the effect of free-stream suppression on the aerodynamic performance of the exhaust system.

GEMINI allows for the direct specification of standard design parameters dictating the geometry of the bypass and core exhaust systems. The design of the upstream duct is carried out by directly specifying the position, slope, and curvature within a series of user defined control points. The core cowl and plug are modeled as straight lines with user specified length and inclination relative to the engine axis. Furthermore, it can be noted that the present design approach includes a third nozzle located on the core cowl, namely the zone 3 vent exhaust. The zone 3 vent is located between the bypass and core nozzles and is used to exhaust various engine cooling and ventilation flows. In terms of parametric design, the user is able to specify the vent exit Mach number as well as its axial position on the core cowl.

2.3 Design Space Exploration (DSE) and optimization

To demonstrate the effectiveness and flexibility of the proposed design methodology, GEMINI has been extended with the development and implementation of a suitable Design Space Exploration (DSE) and optimization environment. The inherently nonlinear nature of the problem tackled in this work, in conjunction with the requirement to mitigate the computational cost associated with numerous CFD simulations, have deemed imperative the compilation of a robust and computationally efficient optimization strategy. Therefore, an integrated optimization framework has been structured and coupled with the developed aerodynamic design method for separate-jet exhausts.

Figure 4 presents an illustration of the computational architecture implemented in the developed optimization framework. The overall approach comprises numerical modules for Design Space Exploration (DSE), Response Surface Modeling (RSM – also known as surrogate modeling), and design optimization. The process of DSE is divided in two main parts; (a) the deployment of a Design of Experiment (DOE) method which aims to explore the available design space, and (b) the construction of Response Surface Models (RSMs) based on the DOE results. To avoid a prohibitively large number of

simulations, it has been decided to build RSMs that can accurately approximate the response of the employed design assessment approach. The RSMs can be subsequently deployed as drivers during the optimization process instead of using time-consuming CFD simulations.

A DOE is a systematic approach to get the maximum amount of system information out of a given number of experiments. Out of the different kinds of DOE available in the literature [44] the Latin Hypercube Design (LHD) algorithm has been selected. The LHD method has been extensively described by Olsson et al. [45]. An RSM essentially constitutes a hyper-surface that describes the mathematical relationship between a set of imposed design inputs and outputs.

Having successfully completed the LHD DOE approach, RSMs can be subsequently structured using the obtained DOE results as model inputs. This process results in the formulation of an analytical model that can predict the aerodynamic response of the nonlinear system in real-time. For the purpose of this work, interpolation using Gaussian Processes Regression [32] (Kriging Interpolation) has been the method of choice to construct RSMs for the exhaust system's performance metrics, C_D and C_V. The classical Leave-One-Out (LOO) cross-validation method [46] is employed to assess the predictive accuracy of the structured RSMs prior to their utilization as predictive tools.

After successful approximation of the simulation method's response to design inputs, the available design space can be systematically explored for potentially optimum solutions. The employed optimization approach has to be immune to the danger of being trapped between locally optimum solutions. Hence, the deployment of a global method is imperative. An established Genetic Algorithm (GA) [47] has been the method of choice for the purpose of this work. GAs are nature-inspired evolutionary algorithms [48]. They imitate biological mutation and natural selection in a simplified way with the purpose of finding the "fittest" solution to multi-dimensional technical problems. Therefore, they do not require computing of the effective sensitivities between design inputs and outputs. As a result, they are immune to the classical weakness of gradient-based methods where the optimization process can be trapped within a locally optimum region close the algorithm's starting point. As such, the overall performance of GAs is not affected by locally optimum solutions.

The combined system outlined above allows for the user to explore the available design space in terms of exhaust system performance for any specified engine cycle. Furthermore, the user can optimize the design of the exhaust system for any performance metric of interest (C_D^{Bypass}, $C_V^{Overall}$, F_G, F_N, etc...).

3 Results and discussion

3.1 Definition of baseline engines

The developed numerical approach has been applied to optimize the Low-Pressure (LP) exhaust system design and core afterbody aerolines for two civil aero-engines. The investigated configurations have been defined in order to be representative of future ($E1$) and current ($E2$) large turbofan engines. The employed thermodynamic cycles have been been structured using publicly available information [49]. The assumed values of BPR are of the order of 15+ and 11 for the future ($E1$) and current ($E2$) engine architecture, in that order. The incorporated cycle parameters in terms of OPR, TET, and component efficiencies have been selected according to the corresponding technology levels using the design guidelines provided in Refs. [3, 50]. Each cycle has been optimized in terms of FPR on the basis of maximizing specific thrust [3].

The 2D axi-symmetric geometries corresponding to the baseline engine models are shown in Fig. 5. The baseline intake, nacelle, and exhaust system geometries have been designed using information found in the public domain combined with engineering judgment. Numerical predictions have been carried out at DP mid-cruise conditions considering both engine models. The corresponding bypass and core nozzle pressure ratios, intake Mass Flow Capture Ratio (MFCR), and free-stream conditions are presented in Table 1. These correspond to the boundary conditions specified for the computations carried out and presented in this section. The associated flow-field solutions for the established baseline engine designs are presented in Figs 6(a) and (b) for the future ($E1$) and current engine architectures ($E2$), respectively. It can be observed that for cruising flight, the bypass exhaust nozzle operate under choked conditions considering both engine models. However, due to the lower values of NPR as shown in Table 1, the core nozzle appears to be unchoked during mid-cruise conditions. This characteristic applies for both engine designs.

3.2 Parametric design space definition

To establish a clear definition of the available design space, the bypass exhaust and core afterbody aerolines of the baseline $E1$ and $E2$ engine architectures (Fig. 5), have been reduced to parametric CST representations through the methodology developed by the authors in Ref. [35]. The conceived design space comprises a total of 11 and 12 design variables for the future ($E1$) and current ($E2$) engine configurations, respectively. Figure 7 provides an illustrative description of the parametric design space established for the $E2$ engine (Fig. 7(b)). All design variables corresponding to axial or radial dimensions are normalized with a reference length as annotated in Fig. 7. All curvature radii are normalized with CP height h_1. The mathematical definition of each design variable is noted in Fig. 7. A similar parametric design space has been defined for the $E1$ engine.

It can be observed from Fig. 7 that the employed design space comprises variables controlling the design of the bypass duct (y_{bp}^{out}, y_{bp}^{in}), exhaust nozzle (A_{ratio}, κ_{len}^{in}, θ_{CP}^{out}, κ_{CP}^{in}, κ_{CP}^{out}, θ_{nozzle}^{out}), core cowl/afterbody (l_{cr}^{cowl}, θ_{cr}^{cowl}), and zone 3 vent (l_{z3}^{exit},M_{z3}^{exit}). It is noted that θ_{nozzle}^{out} is kept constant for the case corresponding to the future engine architecture $E1$. A comprehensive description of the established design space has been provided by the authors in Ref. [35].

3.3 Design space exploration

After establishing a parametric representation of the design space, the developed approach was deployed to investigate the aerodynamic behavior of both engine exhaust systems throughout their respective domains. Each design space was discretized with the deployment of the LHD method. A database containing approximately 360 exhaust geometries was compiled for each engine using the CFD approach described and validated by the authors in Ref. [35]. The correlation between the imposed design variables and the associated performance metrics was subsequently investigated.

Figure 8 presents the correlation matrices obtained through systematic exploration of the design space for both engine architectures. The presented matrices comprise the linear correlation coefficients, also known as Pearson's product-moment of correlation [51], that relate the imposed design variables (Fig. 7) to the performance metrics of interest. The principal linear correlation coefficients indicate the amount and type of average dependency between two specified parameters. A

correlation coefficient can range from -1 to 1. A positive and a negative nonzero value will indicate a direct and an indirect correlation, respectively.

The computed results are presented in the form of Hinton diagrams. Hinton diagrams can be useful in visualizing numerical data in linear algebra, particularly considering weighting or correlation matrices. The presented illustrations demonstrate the distribution of Pearson's product-moment of correlation between the available design variables (Fig. 7) and the performance metrics of interest. Results are presented for the $E1$ and $E2$ engine architectures in Figs. 8(a) and (b), respectively.

Figure 8(a) shows that, with respect to the $E1$ engine, the dominant design parameters that affect C_D^{Bypass} are the nozzle length ratio κ_{len}^{in} (Fig. 7(c)) and the core cowl angle θ_{cr}^{cowl} (Figs. 7(f) and (i)). Specifically, the obtained results suggest that good performance in terms of C_D^{Bypass} requires increased values of length ratio κ_{len}^{in} along with low core cowl angles θ_{cr}^{cowl}. In terms of $C_V^{Overall}$, Fig. 8(a) shows that the dominant design parameter is the outer aeroline slope at the charging plane θ_{CP}^{out} (Fig. 7(d)). The obtained results indicate a positive effect for increased values of θ_{CP}^{out} and vice-versa. The combined influence of C_D^{Bypass} and $C_V^{Overall}$ is also observed in terms of F_G and F_N, which are also strongly affected by κ_{len}^{in}, θ_{cr}^{cowl}, and θ_{CP}^{out}.

A similar behavior can be observed in Fig. 8(b) with respect to exhaust system performance of the $E2$ engine. The dominant design variables are the same as those identified for the $E1$ engine, namely; κ_{len}^{in}, θ_{cr}^{cowl}, and θ_{CP}^{out}. However, the principal parameter that affects C_D^{Bypass} is θ_{CP}^{out} (Fig. 7(d)) with κ_{len}^{in} (Fig. 7(c)) assuming a secondary role. Thus, although the polarity of the effect of the two variables is the same as for the $E1$ engine, their relative impact on C_D^{Bypass} is different. A similar observation applies for $C_V^{Overall}$ where the dominant design parameter is κ_{len}^{in} whilst θ_{CP}^{out} becomes secondary. Furthermore, increasing the core cowl angle θ_{cr}^{cowl} (Figs. 7(f) and (i)) has an adverse effect on both C_D^{Bypass} and $C_V^{Overall}$ with an analogous influence on F_N. It is interesting to note that the computed value for the correlation coefficient that relates F_N to θ_{cr}^{cowl} is roughly -0.62 for both engine architectures. This is attributed to separation losses that may occur on the core cowl for increasing θ_{cr}^{cowl} beyond a minimum value.

Figures 8(a) and (b) demonstrate that nearly identical correlation coefficients have been identified for F_G and F_N. This observation is valid with respect to both engine architectures. This indicates that, within the range of assumptions made for the purpose of this work, the aerodynamic performance of the exhaust system is essentially decoupled from that of the intake and the nacelle forebody. In other words, changes applied to the design of the exhaust system are not expected to influence either the performance of the intake nor that of the nacelle forebody.

3.4 Response surface (surrogate) modeling

The developed approach for Design Space Exploration (DSE) has been extended with the implementation of a suitable surrogate modeling method. The overall formulation is able to utilize the available DOE data to structure models (RSMs) that can approximate the response of the design space with sufficient accuracy. The employed approach is based on interpolation using Gaussian Processes Regression [32] (Kriging Interpolation) for the numerical construction of the required RSMs. A quadratic regression function is employed in the surrogate modeling process along with a squared-exponential auto-

correlation function.

A comprehensive approach has been implemented to assess the quality of the derived surrogate models. The employed formulation is based on the classical Leave-One-Out (LOO) cross-validation method [46] and is applied as follows; A separate surrogate model is created for each of the N data point within the available DOE sample. To derive each individual surrogate model the LOO method employs all available data points apart from the one point for which each individual RSM is derived. Subsequently, the data point left-out of the database is compared against predictions made with its corresponding RSM considering the design that the particular data point represents. This process is repeated for each of the N data points available within the overall sample. To obtained surrogate model predictions are then correlated against the respective data points in terms of Pearson's product moment of correlation along with gradient of the associated linear regression line. Finally, the method also assesses the average model error along with its standard deviation throughout the overall design space for each performance metric of interest.

Figures 9 and 10 present comparisons between surrogate model predictions and direct CFD results for C_D^{Bypass} and $C_V^{Overall}$. Results are presented for the $E1$ and $E2$ engine architectures in Figs. 9 and 10, respectively. A perfectly linear correlation corresponds to a Pearson's index of unity and a regression line gradient equal to 45°. Good correlation can generally be observed for both performance metrics considering both engine architectures. With respect to the $E1$ engine model, the computed correlation coefficients between CFD results and RSM predictions are of the order of 0.97 and 0.87 for C_D^{Bypass} and $C_V^{Overall}$, respectively. A similar level of modeling accuracy is observed for the $E2$ engine case where the corresponding Pearson's indices for C_D^{Bypass} and $C_V^{Overall}$ are of approximately 0.97 and 0.92, in that order.

It can be noticed that Pearson's index for $C_V^{Overall}$ is lower by 0.05–0.1 compared to its reciprocal value for C_D^{Bypass}. This behavior can be observed for both engine models and is an indication of the highly non-linear behavior that $C_V^{Overall}$ exhibits compared to C_D^{Bypass}. It is believed that using a larger number of data points may improve the correlation coefficient for $C_V^{Overall}$ up to a level similar to that of C_D^{Bypass}. The associated gradients of the linear regression lines for C_D^{Bypass} are very close to the 45° whilst the reciprocal slopes for $C_V^{Overall}$ are closer to 43.8°.

Table 2 presents a quantitative assessment of the surrogate modeling error in terms of its mean percentage value $\varepsilon(\%)$ and its standard deviation $\sigma(\%)$ for both engine models. Results are presented for C_D^{Bypass}, $C_V^{Overall}$, and F_N. It can be observed that the structured surrogate models exhibit good predictive qualities in terms of low average percentage errors ε and standard deviation σ when compared to direct CFD predictions. However, it is important to note that the standard deviation of error σ is of the same order of magnitude its average value ε. This implies that the RSM error is widely scattered throughout the design space and can vary consistently. This observation is valid considering both engines and for all performance metrics of interest. This indicates the inherent non-linearity of the investigated systems as well as the difficulty that can be encountered in trying to approximate their response through a surrogate model.

Furthermore, it can be observed that the surrogate modeling error quantities, ε and σ, for C_D^{Bypass} and $C_V^{Overall}$ corresponding to the $E2$ engine are approximately larger by a factor of 2 compared to that estimated for the $E1$ design. However, this is not an indication of insufficiently accurate modeling. Instead, it is attributed to the wider range noted in the variation of both metrics for the $E2$ engine case, compared to the $E1$ design. This has been elaborated in detail by the authors in

Ref. [35]. However, the average error for $C_V^{Overall}$, which is the main metric of interest, is less than an order of magnitude below the overall range observed in the obtained DOE results as shown in Ref. [35].

The above demonstrate the potential of the proposed surrogate modeling approach to approximate the response of the investigated design space with sufficient accuracy. It is emphasized that, since the employed modeling method is based on a regression function applied to an existing database (Kriging interpolation [32]), it is expected that a larger number of data points may effectively result in more accurate surrogate models.

3.5 Exhaust system design optimization

Having cross-validated the derived surrogate models and gained confidence in their predictive accuracy, they can be employed as drivers in a suitable optimization process. The objective is to construct an integrated computational approach that can be used to derive optimum designs for separate-jet exhausts in terms of any defined performance metric. The developed methodology has therefore been extended with the implementation of a global optimization method based on a Genetic Algorithm (GA – Evolutionary method) [47, 48].

The main benefit from using RSMs for the optimization process stems from the very small computational time involved. This allows to derive optimum designs for various objective functions almost instantly. Its is noted that the RSM LOO cross-validation process showed that the associated Pearson's moments of correlation and regression line gradients are close to 1.0 and 45°, respectively, for all metrics of interest. Therefore, the structured RSMs are expected to act as adequate drivers in terms of indicating the location of potentially optimum solutions with the design space. Furthermore, since the RSM quality check showed that the prediction error is relatively small, it is expected that the optimization will yield designs that do not deviate substantially performance-wise when assessed using direct CFD simulation.

In order to demonstrate the effectiveness of the methodology proposed in this paper, the exhaust systems of the future $E1$ and current $E2$ engines were optimized in terms of $C_V^{Overall}$. The population size was set equal to 10 times the number of design variables for each engine case. This resulted in a population size of 110 and 120 for the $E1$ and $E2$ engine models, respectively. In both cases, the evolutionary process was iterated up to 40 generations resulting in a total of 4400 and 4600 surrogate model evaluations for the $E1$ and $E2$ models, in that order. Finally, a convergence criterion of the order of 10^{-12} was employed with respect to average consecutive mutations per generation.

The numerical process of the evolutionary method (GA) applied to the optimization of $C_V^{Overall}$ is illustrated in Fig. 11. The GA exhibited identical numerical behavior considering both engine cases. Thus, to avoid duplication, Fig. 11 presents the convergence process for the $E1$ engine case only. Results are presented for the associated "fitness" value corresponding to the objective function as defined for each of the optimization carried out. The "worst", "best", "average", and "median" values of the associated fitness are included in Fig. 11 for completeness.

The effectiveness of the deployed GA is evident from the fact that a good solution ("best") is obtained relatively early in the optimization process ($N_{eval} \leq 500$). Further evolutionary computation results in slight but noticeable fitness improvements. The "average" and "median" fitness values exhibit similar numerical behavior, both converging asymptotically towards the "best" identified individual per generation. This suggests that the fitness function of the various population

members is distributed symmetrically around the average fitness value of the corresponding generation. This shows that the sampling method employed within the implemented GA exhibits very good numerical behavior. Furthermore, it indicates that the gene pool becomes continuously narrower as the genetic algorithm progresses, therefore containing predominantly chromosomes with desirable fitness characteristics.

It can also be observed that the gene pool still contains "un-fit" chromosomes as is evident from the results presented in Fig. 11. However, the fact that the "average" and "median" fitness values are almost identical with the "best" solutions for $N_{gen} \geq 1500$, implies that the number of these individuals in the gene pool is indeed very small. It is noted that the numerical evaluations presented above require roughly 8-10 seconds of computational time each on a 3.4 GHZ 8-core CPU workstation.

Table 3 outlines the performance improvement achieved in the metrics of interest (ϕ) through the optimization process. Results are presented in the form of percentage differences between the aerodynamic performance of the optimum ($\phi^{Opt.}$) and baseline exhaust designs ($\phi^{Base.}$). The associated metrics have been evaluated using direct CFD simulations (ϕ_{CFD}). Numerical predictions carried out using the RSMs are also included (ϕ_{RSM}) to assess their predictive accuracy near the optimum design region.

Considering the future $E1$ engine, the optimized exhaust system has been improved by roughly 0.46% and 0.087% in terms of C_D^{Bypass} and $C_V^{Overall}$, respectively, relative to the baseline design. The combined improvement results in a F_G and F_N increase of the order of 0.55% and 1.4%, respectively. With respect to the current $E2$ architecture, a smaller improvement has been obtained with respect to C_D^{Bypass} of 0.29%. However, a significant increase in $C_V^{Overall}$ can be observed that reaches approximately 0.25%. The combined effect leads to an overall F_G and F_N increase of the order of 1.7% and 3.4%, respectively.

The associated flow-field conditions corresponding to the baseline and optimized exhaust designs for the future $E1$ engine design are illustrated in Figs. 12(a) and (b), respectively. It can be observed that the baseline design (Fig. 12(a)) produces a strong normal shock located at approximately 50% of h_2 downstream of the nozzle exit plane. This strong normal shock generates entropy and reduces the jet's total pressure as well as overall F_G. Figure 12(b) shows that the optimization process has implicitly managed to mitigate this undesirable flow feature. This has been achieved by increasing the nozzle length ratio κ_{len}^{in} (Fig. 7(c)) and rearranging the inner line curvature distribution upstream of the nozzle exit plane to accommodate the required flow turning. This adjustment allows the flow to gradually align itself with the core cowl angle θ_{cr}^{cowl} before exhausted to ambient. As a result, flow acceleration to sonic conditions is achieved predominantly through mean flow area reduction, instead of locally induced acceleration due to aeroline curvature. Furthermore, an appropriate value for θ_{CP}^{out} (Fig. 7(d)) has been acquired which effectively minimizes any radial pressure gradients at the CP prior to any flow turning in the downstream exhaust nozzle.

In addition to the above, it can be noted that the optimization has resulted in a duct design that employs a gradual diffusion upstream of the nozzle CP to maintain low wall velocities. This design adjustment effectively reduces skin friction losses throughout the corresponding portion of the bypass duct. The duct subsequently converges up to the nozzle CP where a constant area distribution is applied before the flow enters the convergent nozzle. Regarding the post-nozzle exit components,

the optimized design has a longer core cowl l_{cr}^{cowl} with a lower half-cone angle θ_{cr}^{cowl} and a zone 3 vent location closer to the bypass nozzle exit. The employed design adjustments are in agreement with the computed matrix of correlation coefficients shown in Fig. 8(a).

Figures 13(a) and (b) present the flow-field solutions for the baseline and optimized exhaust designs with respect to the current $E2$ engine. A design approach similar to that employed for the $E1$ engine has been followed with respect to the geometry of the bypass duct. A diverging aeroline pattern has been implemented to maintain low wall velocities and reduce skin-friction losses in bypass duct. However, a different philosophy has been favored compared to the $E1$ engine with respect to the design of the post-nozzle exit components. Specifically, the optimized design has a shorter core cowl l_{cr}^{cowl} with a lower half-cone angle and a zone 3 vent position closer to the core nozzle exit.

The differences observed in the optimum design of the post-nozzle exit components between the two engine architectures are attributed to the different aerodynamic mechanisms that govern the flow behavior on the transonic core cowl. Specifically, the $E2$ design has a lower BPR and higher NPR_{Bypass} compared to $E1$. This results in a strong, complex, and sensitive shock-pattern on the core afterbody as shown in Figs. 13(a) and (b). Due to the high NPR_{Bypass} a region of high-velocity supersonic flow with $M \approx 1.4$ can be observed on the core cowl. This region terminates with a strong normal shock. For the baseline design, this strong normal shock is followed by shock induced separation half-way along the core cowl. This occurs due to the low momentum of the upstream boundary layer that originates from the upstream zone 3 vent exhaust flow. Therefore, the boundary layer on the core cowl for the baseline design is incapable of sustaining high adverse pressure gradients due to the upstream location of the zone 3 vent. The optimization has mitigated this undesirable flow feature by placing the zone 3 vent downstream of the strong normal shock. Although the optimum exhaust design still features a normal shock originating at the exit of the zone 3 vent exhaust, no flow separation occurs on the core cowl.

Hence, it has been shown that the proposed approach is implicitly able to identify and mitigate undesirable flow-features that may compromise the aerodynamic performance of the exhaust system. The design process can be automatically directed towards optimum design regions where adverse flow effects can be eliminated. Thus, the developed method allows to design optimally configured separate-jet exhaust systems for any specified engine architecture.

4 Conclusions

This paper has described an integrated approach targeting the design optimization of separate-jet exhaust systems for future civil aero-engines. The employed method consists of numerical modules for cycle analysis, geometry parameterization, mesh generation, and viscous/compressible flow solution. A novel analytical tool based on CST functions has been employed for the parametric geometry definition of the exhaust duct and nozzle components employed in a civil aero-engine installation. A 2D axi-symmetric Reynolds Averaged Navier–Stokes (RANS) CFD modeling approach has been employed for the aerodynamic performance prediction of separate-jet exhaust systems. The employed formulation has been expanded with the implementation of a comprehensive optimization strategy comrpising numerical algorithms for Design of Experiment (DOE), Response Surface Modeling (RSM), and genetic optimization (GA). The developed framework has been used to optimize the exhaust system design for two civil aero-engines, representative of current and future large turbofan architectures,

respectively.

Numerical predictions indicate that the design optimization of the exhaust system could lead to a net propulsive force increase of the order of 1.4% and 3.4% for future and current engine configurations, respectively, relative to a set of notional baseline designs. The overall method has been successful in identifying effective guidelines for the optimum design of separate-jet exhaust systems. It has been shown that the proposed approach is implicitly able to identify and mitigate undesirable flow-features that may compromise the aerodynamic performance of the exhaust system. This allows for the design process to be automatically re-directed towards optimum design regions where the existence of adverse flow effects can be minimized. The developed methodology can be viewed as an enabling technology towards the design of optimally configured exhaust systems, consequently leading to increased overall engine thrust and reduced specific fuel consumption.

5 Acknowledgments

This project was co-funded by Innovate UK. The authors would also like to acknowledge Profs Vassilios Pachidis and Pericles Pilidis from the Propulsion Engineering Centre at Cranfield University, for their insightful advice and continuing support.

References

[1] Clarke, J.-P., "The role of advanced air traffic management in reducing the impact of," *Elsevier Science Ltd*, Vol. 9, No. 5, 2003, pp. 161–165.

[2] Epstein, A. H., "Aeropropulsion for Commercial Aviation in the Twenty-First Century and Research Directions Needed," *AIAA Journal*, Vol. 52, (5), May 2014, pp. 901–911.

[3] Walsh, P. and Fletcher, P., *Gas Turbine Performance Engineering*, Blackwell Publishing, 2004.

[4] Kyprianidis, K. G., Grnstedt, T., Ogaji, S. O. T., Pilidis, P., and Singh, R., "Assessment of Future Aero-engine Designs With Intercooled and Intercooled Recuperated Cores," *ASME*, Vol. 133, (1), April 2010, pp. 011701.

[5] Kyprianidis, K. G., Rolt, A. M., and Grnstedt, T., "Multidisciplinary Analysis of a Geared Fan Intercooled Core Aero-Engine," *ASME J. Eng. Gas Turbines and Power*, Vol. 136, (1), January 2013, pp. 011203.

[6] Kyprianidis, K. G. and Rolt, A. M., "On the Optimization of a Geared Fan Intercooled Core Engine Design," *ASME J. Eng. Gas Turbines and Power*, Vol. 137, (4), April 2014, pp. 041201.

[7] Guha, A., "Optimum Fan Pressure Ratio for Bypass Engines with Separate or Mixed Exhaust Streams," *Journal of Propulsion and Power*, Vol. 17, (5), September-October 2001 2001, pp. 1117–1122.

[8] MIDA, S. G., "Guide to In-Flight Thrust Measurement of Turbojets and Fan Engines," Advisory Group for Aerospace Research and Development, AGARD-AG-237, January 1979.

[9] AGARD, "Aerodynamics of Power Plan Installation," Advisory Group for Aerospace Research and Development, AGARD-CP-301, 7 Rue Ancelle 92200 Newilly, Sur Seine, France, May 1981.

[10] Covert, E. E., James, C. R., Kimsey, W. M., Rickey, G. K., and Rooney, E., *Thrust and Drag: Its Prediction and Verification (Progress in Astronautics and Aeronautics Series)*, American Institute of Aeronautics & Astronautics, Reston, VA 20191-4344, 1985.

[11] Dusa, D., Lahti, D., and Berry, D., "Investigation of Subsonic Nacelle Performance Improvement Concept," 18th Joint Propulsion Conference, Cleveland, OH, U.S.A, June 21-23 1982.

[12] Malecki, R. E. and Lord, K., "Aerodynamic Performance of Exhaust Nozzles Derived from CFD Simulation," American Institute for Aeronautics and Astronautics, AIAA-1995-2623, Reston, VA 20191-4344, 1995.

[13] Decher, R. and Tegeler, D. C., "High Accuracy Force Accounting Procedures for Turbo Powered Simulator Testing," American Institute for Aeronautics and Astronautics, AIAA-1975-1324, Reston, VA 20191-4344, 1975.

[14] Zhang, Y., Chen, H., Zhang, M., Zhang, M., Li, Z., and Fu, S., "Performance Prediction of Conical Nozzle Using Navier-Stokes Computation," *Journal of Propulsion and Power*, Vol. 31, (1), January-February 2015, pp. 192–203.

[15] Zhang, Y., Chen, H., Fu, S., Zhang, M., and Zhang, M., "Drag Prediction Method of Powered-On Civil Aircraft Based on Thrust-Drag Bookkeping," *Chinese Journal of Aeronautics*, Vol. 28, (4), August 2015, pp. 1023–1033.

[16] Heath, C. M., Gray, J. S., Park, M. A., Nielsen, E. J., and Carlson, J.-R., "Aerodynamic Shape Optimization of a Dual-Stream Supersonic Plug Nozzle," SciTech 2015, No. GRC-E-DAA-TN19528, Reston, VA, United States, 5-9 January 2015.

[17] Nielsen, E. J. and Anderson, W. K., "Recent Improvements in Aerodynamic Design Optimization on Unstructured

Meshes," *AIAA Journal*, Vol. 40, (6), June 2002, pp. 1155–1163.

[18] Nielsen, E. J. and Diskins, B., "Discrete Adjoint-Based Design for Unsteady Turbulent Flows on Dynamic Overset Unstructured Grids," *AIAA Journal*, Vol. 51, (6), June 2013, pp. 1355–1373.

[19] Schittkowski, K., "On the Convergence of a Sequential Quadratic Programming Method with an Augmented Lagrangian Search Direction," *Optimization*, Vol. 14, 1983, pp. 197–216.

[20] Clemen, C., Albrecht, P., and Herzog, S., "Systematic Optimisation of a Turbofan Bypass Duct System," ASME Turbo Expo 2012: Turbine Technical Conference and Exposition, No. GT2012-68276, Copenhagen, Denmark, June 11-15 2012.

[21] Lapworth, B. L., "HYDRA-CFD: A Framework for Collaborative CFD Development," International Conference on Scientific and Engineering Computation (IC-SEC), Singapore, June 30-July 02 2004.

[22] Sobol, I. M., "On the Systematic Search in a Hypercube," *Siam J. Numer. Anal.*, Vol. 16, (5), October 1979.

[23] Wright, G. B., *Radial Basis Function Interpolation: Numerical and Analytical Development*, Ph.D. thesis, Department of Applied Mathematics, University of Colorado, USA, 2003.

[24] Sasaki, D., Obayashi, S., and Nakahashi, K., "Navier-Stokes Optimization of Supersonic Wings with Four Objectives Using Evolutionary Algorithm," *Journal of Aircraft*, Vol. 39, (4), July-August 2002, pp. 621–629.

[25] Haderlie, J. and Crossley, W., "Multiobjective Optimization of a Supersonic-Inlet Bypass Duct Splitter via Surrogate Modeling," 13th AIAA/ISSMO Multidisciplinary Analysis Optimization Conference, Fort Worth, Texas, September 13-15 2010.

[26] Kulfan, B. M. and Bussoletti, J. E., ""Fundamental" Parametric Geometry Representations for Aircraft Component Shapes," 11th AIAA/ISSMO Multidisciplinary Analysis and Optimization Conference, Portsmouth, Virginia, September 2006.

[27] Ceze, M., Hayashi, M., and Volpe, E., "A Study of the CST Parameterization Characteristics," 27th AIAA Applied Aerodynamics Conference, No. AIAA 2009-3767, San Antonio, Texas, 22-25 June 2009.

[28] Kulfan, B. M., "A Universal Parametric Geometry Representation Method CST," 45th AIAA Aerospace Sciences Meeting and Exhibit, Reno Hilton, Reno, Neva, January 8-11 2007.

[29] Kulfan, B. M., "Recent Extensions and Applications of the 'CST' Universal Parametric Geometry Representation Method," *Aeronautical Journal*, Vol. 114, (1153), March 2010, pp. 157–176.

[30] Forrester, A. I. J., Sobester, A., and Keane, A. J., *Engineering Design via Surrogate Modelling: A Practical Guide*, John Wiley & Sons, Inc., Chichester, UK, 2008.

[31] Krige, D. G., "A Statistical Approach to Some Basic Mine Valuation Problems on the Witwaterstrand," *Journal of the Chemical, Metallurgical and Mining Society of South Africa*, Vol. 52, (6), December 1951, pp. 119–139.

[32] Bayraktar, H. and Turalioglu, F., "A Kriging-based approach for locating a sampling site in the assessment of air quality," *Stochastic Environmental Research and Risk Assessment*, Vol. 19, 2005, pp. 301–305.

[33] Qiu, S., Song, W. B., and Liu, H., "Shape Optimization of a General Bypass Duct for Tone Noise Reduction Using Continuous Adjoint Method," *IMECHE Journal of Mechanical Engineering Science*, Vol. 228, (1), January 2014,

pp. 119–134.

[34] Wu, H. Y., Yang, S. C., and Liu, F., "Comparison of Three Geometric Representations of Airfoils for Aerodynamic Optimisation," 16th AIAA Computational Fluid Dynamics Conference, Orlando, FL, June 23-26 2003.

[35] Goulos, I., Stankowski, T., Otter, J., MacManus, D., Grech, N., and Sheaf, C., "Aerodynamic Design of Separate-Jet Exhausts for Future Civil Aero-Engine, Part 1: Parametric Geometry Definition and CFD Approach," *ASME J. Eng. Gas Turbines and Power*, 2015 (submitted).

[36] Macmillan, W. L., *Development of a Module Type Computer Program for the Calculation of Gas Turbine Off Design Performance*, Ph.D. thesis, Department of Power and Propulsion, Cranfield University, 1974.

[37] Kulfan, B. M., "Universal Parametric Geometry Representation Method," *Journal of Aircraft*, Vol. 45, (1), January-February 2008, pp. 142–158.

[38] Zhu, F. and Qin, N., "Intuitive Class/Shape Function Parameterization for Airfoils," *AIAA Journal*, Vol. 52, (1), January 2014, pp. 17–25.

[39] Ansys Inc., 275 Technology Drive, Canonsburg, PA 15317, *ANSYS ICEM CFD Tutorial Manual*.

[40] Ansys Inc., 275 Technology Drive, Canonsburg, PA 15317, *ANSYS FLUENT User's Guide*.

[41] Li, Y. G., Marinai, L., Gatto, E. L., Pachidis, V., and Pilidis, P., "Multiple-Point Adaptive Performance Simulation Tuned to Aeroengine Test-Bed Data," *Journal of Propulsion and Power*, Vol. 25, (3), 2009, pp. 635–641.

[42] Pachidis, V., Pilidis, P., Marinai, L., and Templalexis, I., "Towards a full two dimensional gas turbine performance simulator," *Aeronautical Journal*, Vol. 111, (1121), 2007, pp. 433–442.

[43] Lee, Y.-S., Ma, Y., and Jegadesh, G., "Rolling-Ball Method and Contour Marching Approach to Identifying Critical Regions for Complex Surface Machining," *Computers in Industry*, Vol. 41, (2), March 2000, pp. 163–180.

[44] Lorenzen, T. and Anderson, V., *Design of Experiments: A No-Name Approach*, CRC Press, 1993.

[45] Olsson, A., Sandberg, G., and Dahlblom, O., "On Latin hypercube sampling for structural reliability analysis," *Structural Safety*, Vol. 25, No. 1, 2003, pp. 47 – 68.

[46] Kohavi, R., "A Study of Cross-Validation and Bootstrap for Accuracy Estimation and Model Selection," Proceedings of the Fourteenth International Joint Conference on Artificial Intelligence, Vol. 2, 1995, p. 11371143.

[47] Schwefel, H., *Numerical optimization of computer models*, Interdisciplinary systems research, Wiley, 1981.

[48] Haupt, R. L. and Haupt, S. E., *Practical Genetic Algorithms, 2nd edition*, John Wiley & Sons, Inc., Hoboken, New Jersey, US, 2004.

[49] Gunston, B., *Jane's Aero-engines*, Jane's Information Group, 1996.

[50] Mattingly, J., *Elements of gas turbine propulsion*, No. v. 1 in McGraw-Hill series in mechanical engineering, McGraw-Hill, 1996.

[51] Hotelling, H., "New Light in the Correlation Coefficient and its Transforms," *Journal of the Royal Statistical Society*, Vol. 15, (2), No. 193-232, 1953.

List of Figures

1 Notionally defined axi-symmetric geometry for a Very-High Bypass Ratio (VHBR) turbofan engine with separate-jet exhausts . . . 25

2 Upper-level overview of the developed software architecture . . . 26

3 Geometric design approach employed in GEMINI . . . 27

4 Developed framework for design space exploration and optimisation . . . 28

5 2D axi-symmetric geometries of investigated engine architectures: (a) Design representative of future engine architectures ($E1$), (b) Design representative of current engine architectures ($E2$) . . . 29

6 Mach number contours for the baseline exhaust system designs at DP mid-cruise conditions: (a) Design representative of future engine architectures ($E1$), (b) Design representative of current engine architectures ($E2$) . . . 30

7 Design space definition: (a) Bypass duct outer line position $y_{bp}^{out} = \frac{R_{bp}^{out}}{L_{duct}^{in}}$, (b) $y_{bp}^{in} = \frac{R_{bp}^{in}}{L_{duct}^{in}}$, (c) Nozzle CP to exit area ratio $A_{ratio} = \frac{A_{CP}}{A_{exit}}$ and length ratio $\kappa_{len}^{in} = \frac{L_{in}^{Nozzle}}{h_2}$, (d) Outer line slope at the CP θ_{CP}^{out}, (e) CP inner/outer curvature radius ratio $\kappa_{CP}^{in/out} = \frac{R_{curve}^{CP,in/out}}{h_2}$, (f) Core cowl length $l_{cr}^{cowl} = \frac{L_{cr}^{cowl}}{R_{fan}}$, (g) Zone 3 vent exit position $l_{z3}^{exit} = \frac{L_{z3}^{exit}}{L_{cr}^{cowl}}$, (h) Zone 3 exit Mach no. M_{z3}^{exit}, (i) Core cowl angle θ_{cr}^{cowl} and outer line angle θ_{nozzle}^{out} . 31

8 Linear correlation estimation between design variables and performance metrics: (a) future $E1$ engine, (b) current $E2$ engine . . . 32

9 Leave-One-Out (LOO) cross-validation applied to the structured surrogate models for the $E1$ future engine model: (a) Bypass nozzle discharge coefficient C_D^{Bypass}, (b) Overall thrust coefficient $C_V^{Overall}$ . . . 33

10 Leave-One-Out (LOO) cross-validation applied to the structured surrogate models for the $E2$ current engine model: (a) Bypass nozzle discharge coefficient C_D^{Bypass}, (b) Overall thrust coefficient $C_V^{Overall}$ . . . 34

11 Evolutionary computation for the optimization of $C_V^{Overall}$ – convergence process . . . 35

12 Comparison between baseline and optimum exhaust designs for the future $E1$ engine architecture: (a) Baseline exhaust design, (b) Exhaust design optimized for $C_V^{Overall}$ . . . 36

13 Comparison between baseline and optimum exhaust designs for the current $E2$ engine architecture: (a) Baseline exhaust design, (b) Exhaust design optimized for $C_V^{Overall}$ . . . 37

List of Tables

1 Engine operating conditions used for Design Space Exploration 22

2 Quality assessment of the derived surrogate models 23

3 Comparison between optimum and baseline exhaust designs 24

Journal of Engineering for Gas Turbines and Power. Received November 22, 2015;
Accepted manuscript posted February 1, 2016. doi:10.1115/1.4032652
Rolls-Royce plc

Table 1. Engine operating conditions used for Design Space Exploration

Cycle parameter.	$E1$	$E2$	Unit
$\left(\frac{P_0^{inlet}}{P_{st}^{amb}}\right)^{Bypass}$	2.2	2.8	–
$\left(\frac{P_0^{inlet}}{P_{st}^{amb}}\right)^{Core}$	1.5	1.4	–
$MFCR^{intake}$	0.7	0.6	–
BPR	15+	11	–
M_∞	0.85	0.85	–
Altitude	10668	13106	m
Rated cruise F_N	$\approx$60	$\approx$40	kN

Journal of Engineering for Gas Turbines and Power. Received November 22, 2015;
Accepted manuscript posted February 1, 2016. doi:10.1115/1.4032652
Rolls-Royce plc

Table 2. Quality assessment of the derived surrogate models

Metric	Avg. error ε (%)	Std. deviation σ (%)
$E1$ engine		
C_D^{Bypass}	0.076	0.058
$C_V^{Overall}$	0.016	0.019
F_N	0.567	0.545
$E2$ engine		
C_D^{Bypass}	0.134	0.245
$C_V^{Overall}$	0.041	0.037
F_N	0.435	0.542

Journal of Engineering for Gas Turbines and Power. Received November 22, 2015;
Accepted manuscript posted February 1, 2016. doi:10.1115/1.4032652
Rolls-Royce plc

Table 3. Comparison between optimum and baseline exhaust designs

ϕ	$\frac{\phi_{CFD}^{Opt.} - \phi_{RSM}^{Opt.}}{\phi_{CFD}^{Opt.}}$	(%)	$\frac{\phi_{CFD}^{Opt.} - \phi_{CFD}^{Base.}}{\phi_{CFD}^{Base.}}$	(%)
$E1$				
C_D^{Bypass}	-0.12		0.46	
$C_V^{Overall}$	-0.08		0.087	
F_G (N)	-0.54		0.55	
F_N (N)	–		1.4	
$E2$				
C_D^{Bypass}	-0.03		0.29	
$C_V^{Overall}$	-0.17		0.25	
F_G (N)	-1.4		1.7	
F_N (N)	-2.4		3.4	

Journal of Engineering for Gas Turbines and Power. Received November 22, 2015;
Accepted manuscript posted February 1, 2016. doi:10.1115/1.4032652
Rolls-Royce plc

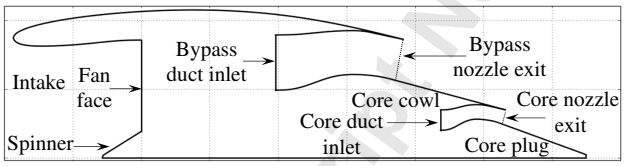

Fig. 1. Notionally defined axi-symmetric geometry for a Very-High Bypass Ratio (VHBR) turbofan engine with separate-jet exhausts

Journal of Engineering for Gas Turbines and Power. Received November 22, 2015;
Accepted manuscript posted February 1, 2016. doi:10.1115/1.4032652
Rolls-Royce plc

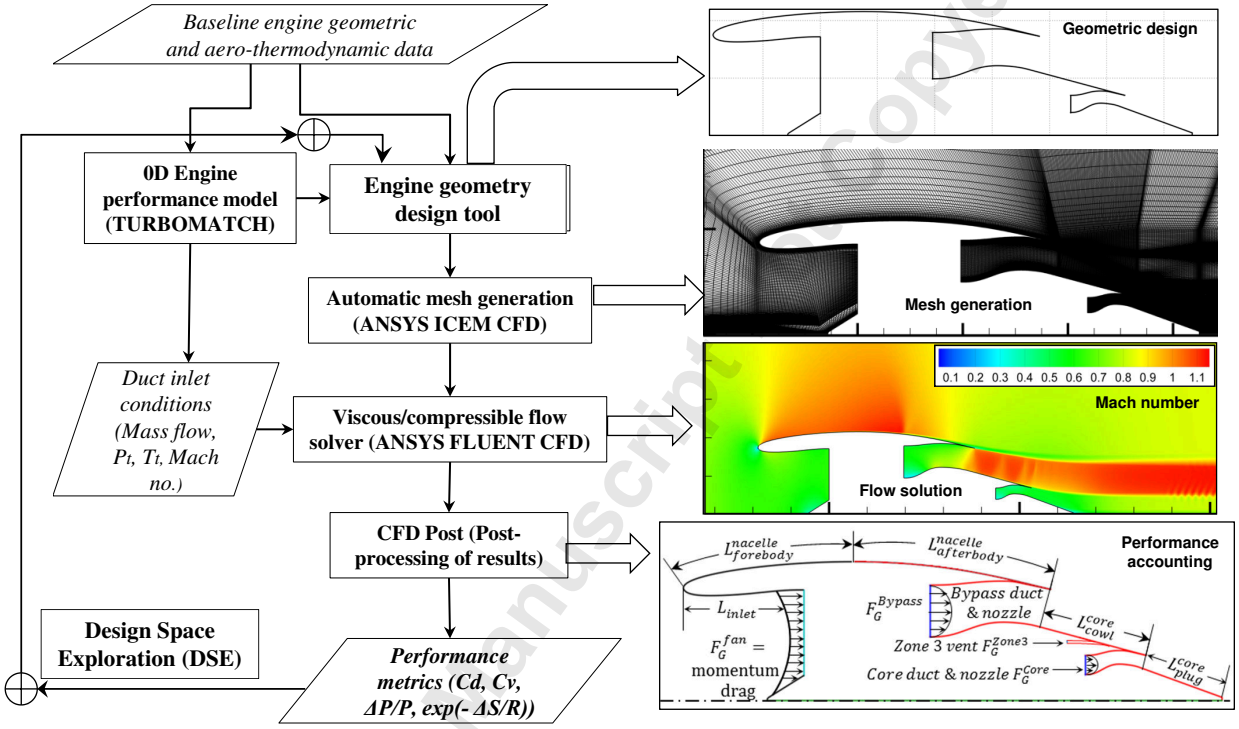

Fig. 2. Upper-level overview of the developed software architecture

Journal of Engineering for Gas Turbines and Power. Received November 22, 2015;
Accepted manuscript posted February 1, 2016. doi:10.1115/1.4032652
Rolls-Royce plc

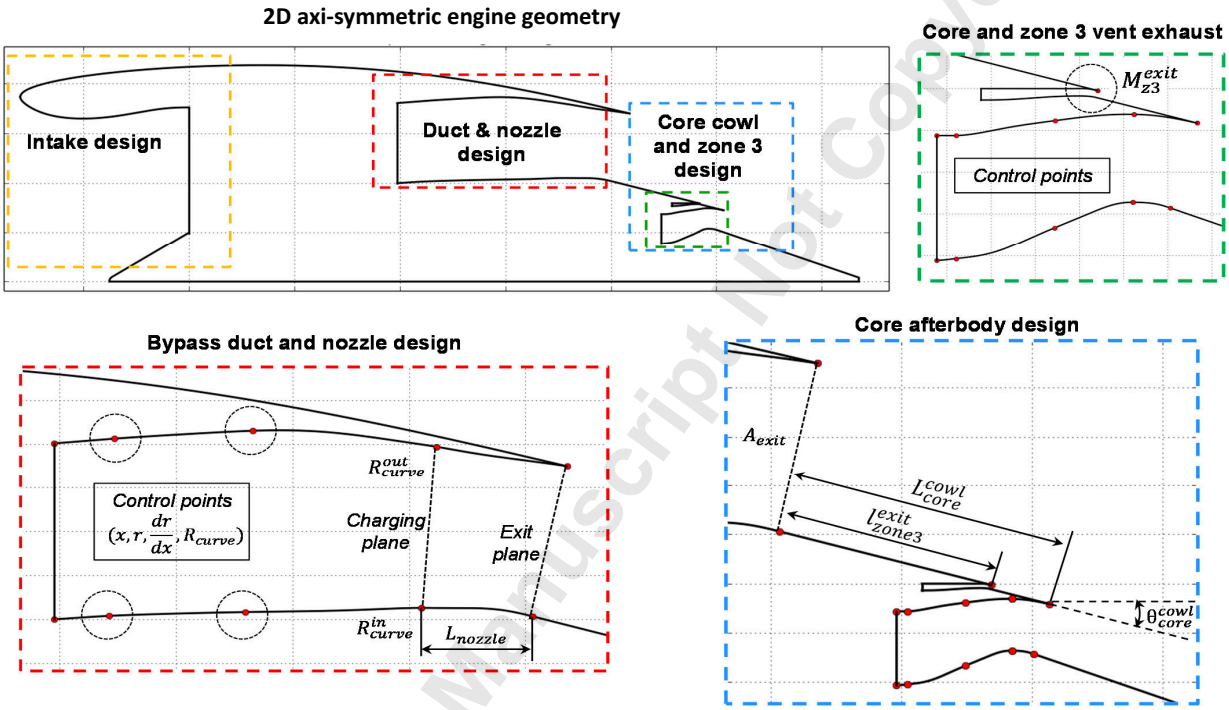

Fig. 3. Geometric design approach employed in GEMINI

Journal of Engineering for Gas Turbines and Power. Received November 22, 2015;
Accepted manuscript posted February 1, 2016. doi:10.1115/1.4032652
Rolls-Royce plc

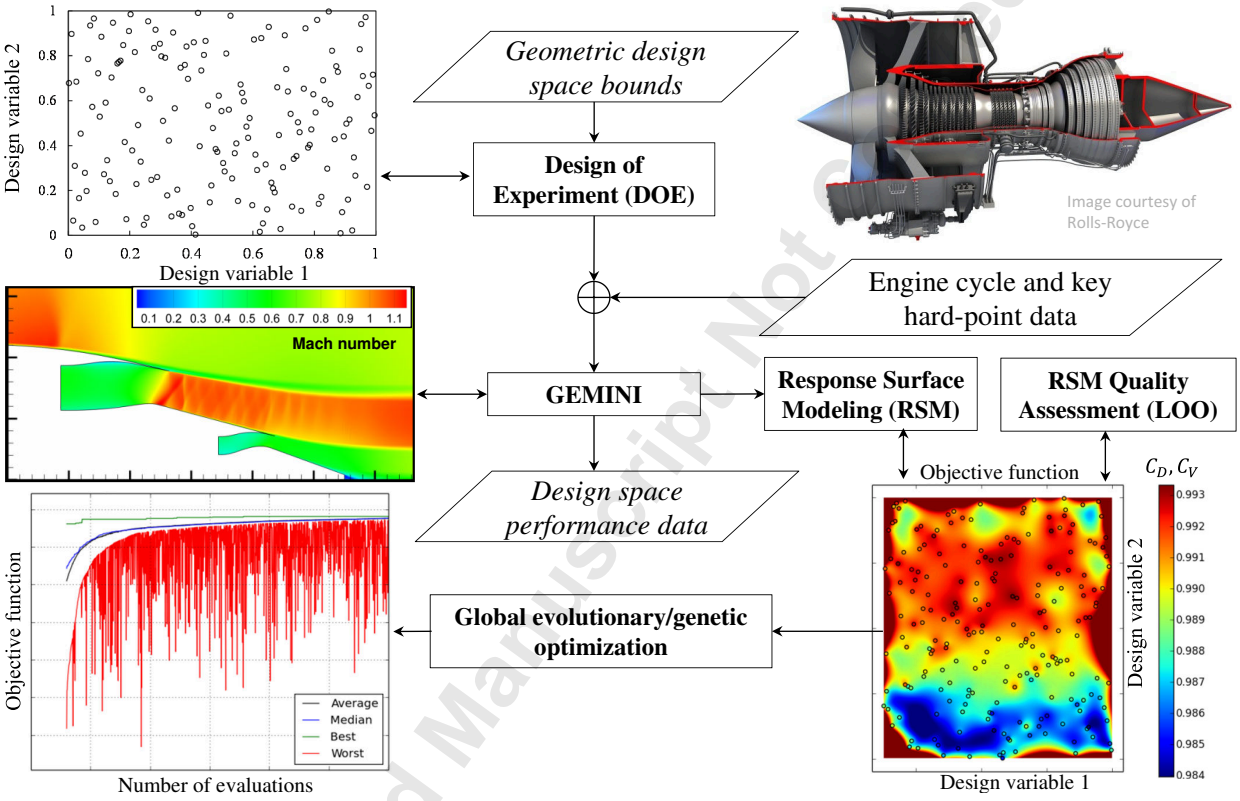

Fig. 4. Developed framework for design space exploration and optimisation

Journal of Engineering for Gas Turbines and Power. Received November 22, 2015;
Accepted manuscript posted February 1, 2016. doi:10.1115/1.4032652
Rolls-Royce plc

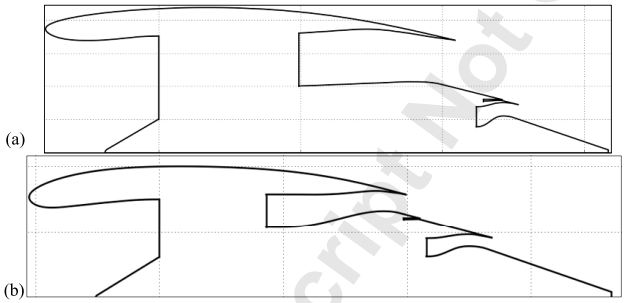

Fig. 5. 2D axi-symmetric geometries of investigated engine architectures: (a) Design representative of future engine architectures ($E1$), (b) Design representative of current engine architectures ($E2$)

Journal of Engineering for Gas Turbines and Power. Received November 22, 2015;
Accepted manuscript posted February 1, 2016. doi:10.1115/1.4032652
Rolls-Royce plc

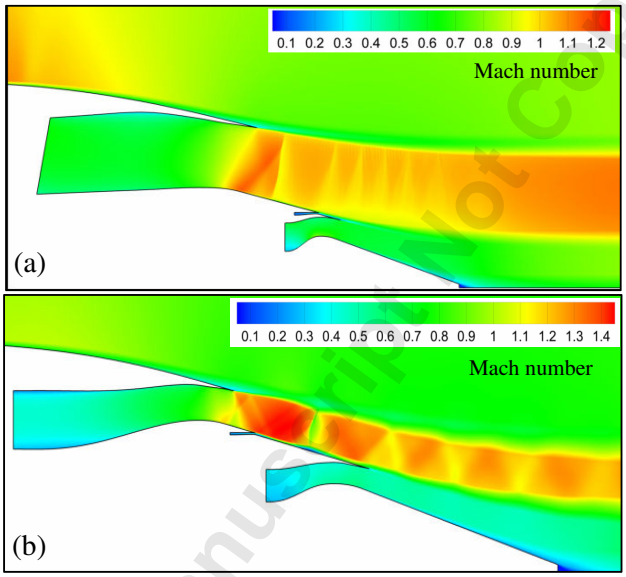

Fig. 6. Mach number contours for the baseline exhaust system designs at DP mid-cruise conditions: (a) Design representative of future engine architectures ($E1$), (b) Design representative of current engine architectures ($E2$)

Journal of Engineering for Gas Turbines and Power. Received November 22, 2015;
Accepted manuscript posted February 1, 2016. doi:10.1115/1.4032652
Rolls-Royce plc

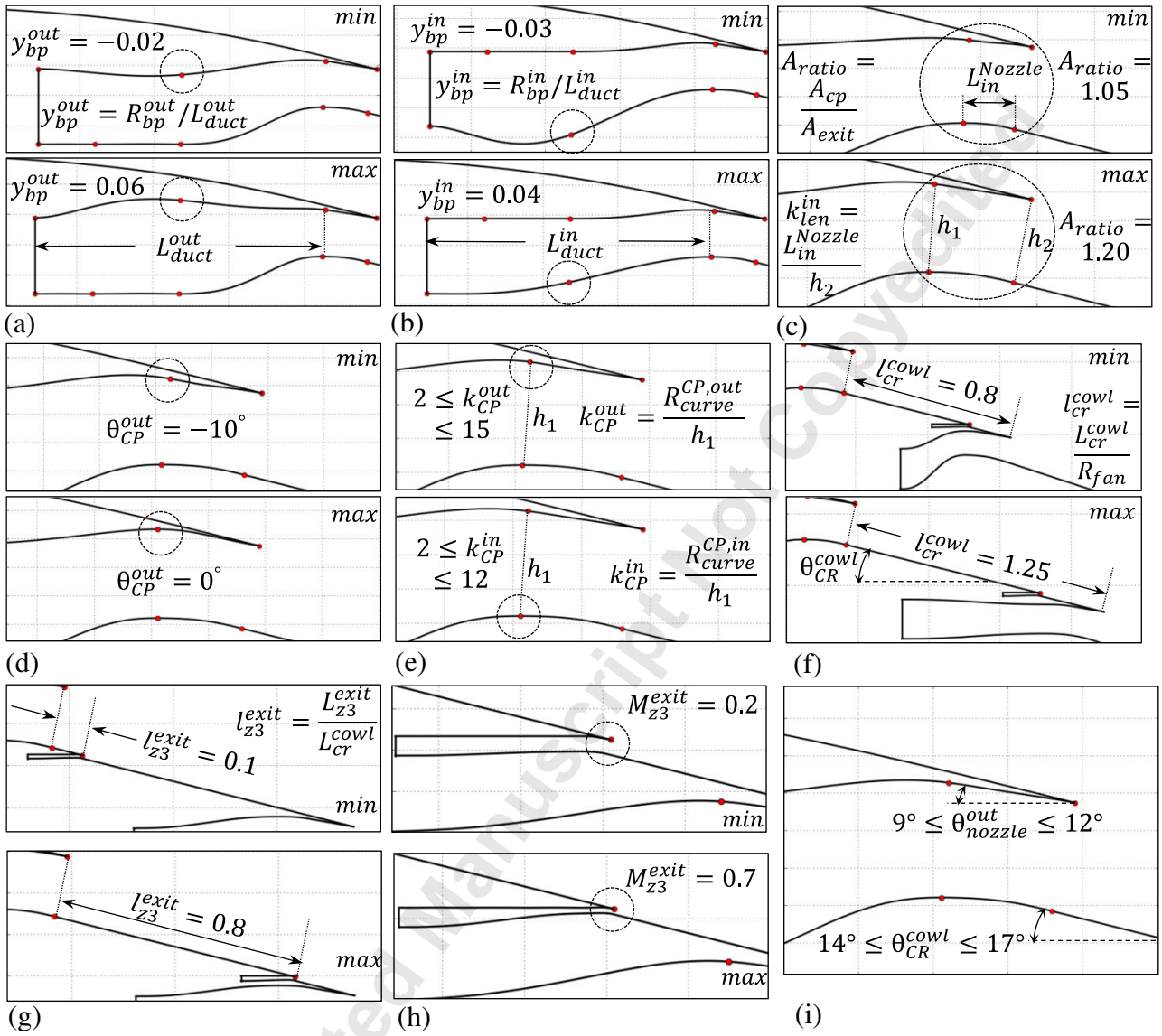

Fig. 7. Design space definition: (a) Bypass duct outer line position $y_{bp}^{out} = \frac{R_{bp}^{out}}{L_{duct}^{in}}$, (b) $y_{bp}^{in} = \frac{R_{bp}^{in}}{L_{duct}^{in}}$, (c) Nozzle CP to exit area ratio $A_{ratio} = \frac{A_{CP}}{A_{exit}}$ and length ratio $\kappa_{len}^{in} = \frac{L_{in}^{Nozzle}}{h_2}$, (d) Outer line slope at the CP θ_{CP}^{out}, (e) CP inner/outer curvature radius ratio $\kappa_{CP}^{in/out} = \frac{R_{curve}^{CP,in/out}}{h_2}$, (f) Core cowl length $l_{cr}^{cowl} = \frac{L_{cr}^{cowl}}{R_{fan}}$, (g) Zone 3 vent exit position $l_{z3}^{exit} = \frac{L_{z3}^{exit}}{L_{cr}^{cowl}}$, (h) Zone 3 exit Mach no. M_{z3}^{exit}, (i) Core cowl angle θ_{cr}^{cowl} and outer line angle θ_{nozzle}^{out}

Journal of Engineering for Gas Turbines and Power. Received November 22, 2015;
Accepted manuscript posted February 1, 2016. doi:10.1115/1.4032652
Rolls-Royce plc

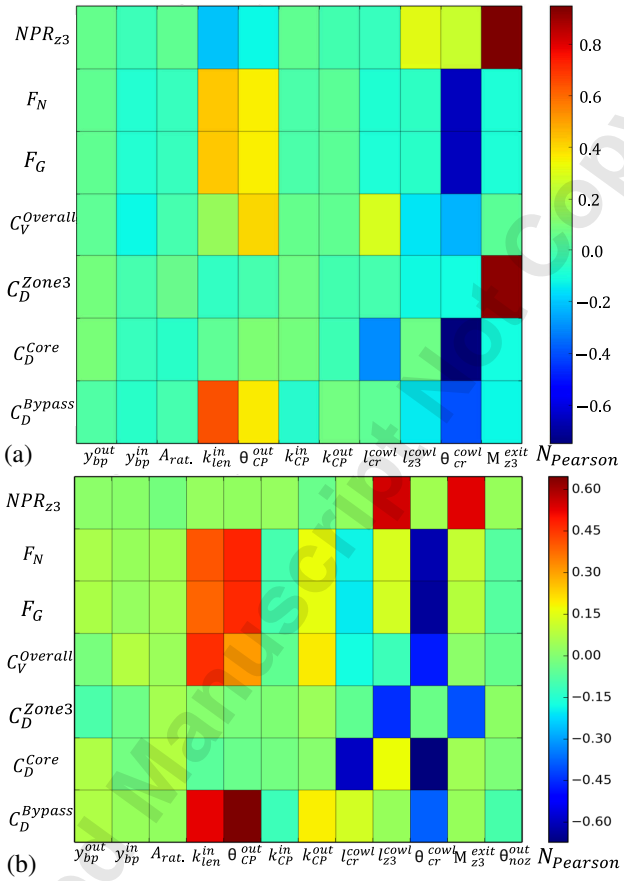

Fig. 8. Linear correlation estimation between design variables and performance metrics: (a) future $E1$ engine, (b) current $E2$ engine

Journal of Engineering for Gas Turbines and Power. Received November 22, 2015;
Accepted manuscript posted February 1, 2016. doi:10.1115/1.4032652
Rolls-Royce plc

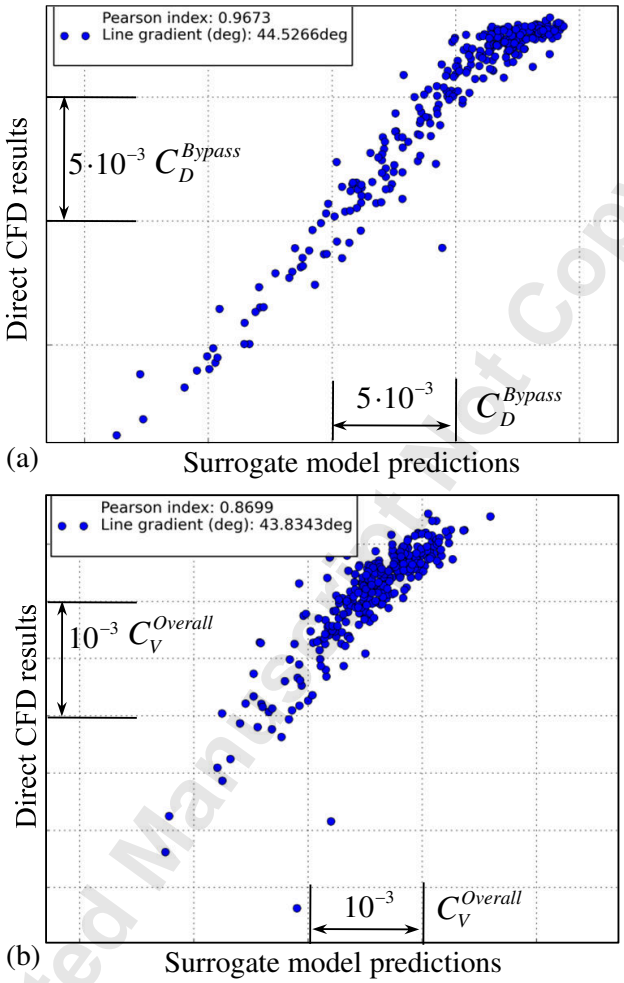

Fig. 9. Leave-One-Out (LOO) cross-validation applied to the structured surrogate models for the $E1$ future engine model: (a) Bypass nozzle discharge coefficient C_D^{Bypass}, (b) Overall thrust coefficient $C_V^{Overall}$

Journal of Engineering for Gas Turbines and Power. Received November 22, 2015;
Accepted manuscript posted February 1, 2016. doi:10.1115/1.4032652
Rolls-Royce plc

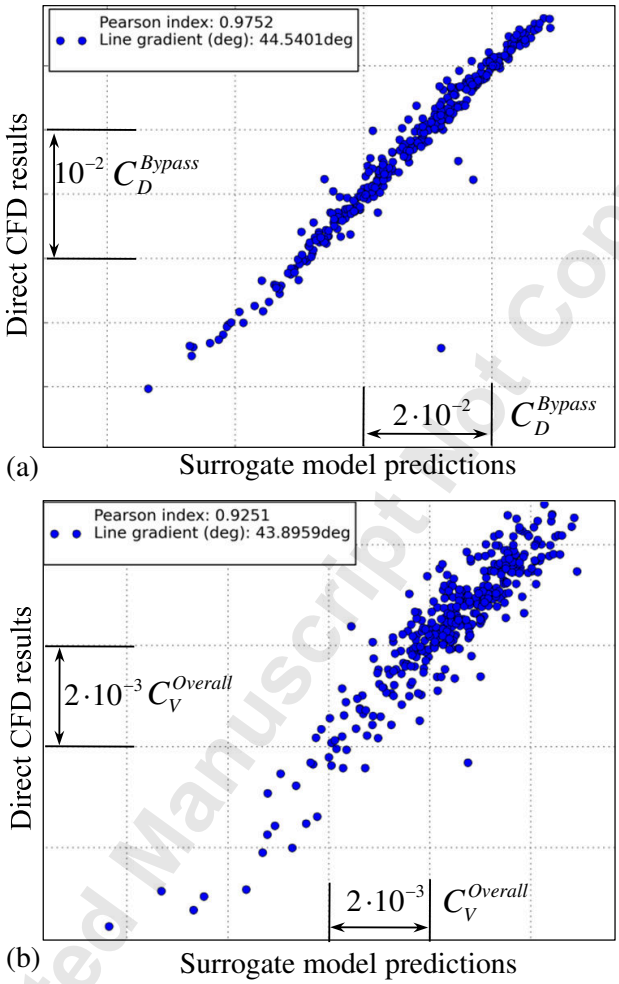

Fig. 10. Leave-One-Out (LOO) cross-validation applied to the structured surrogate models for the $E2$ current engine model: (a) Bypass nozzle discharge coefficient C_D^{Bypass}, (b) Overall thrust coefficient $C_V^{Overall}$

Journal of Engineering for Gas Turbines and Power. Received November 22, 2015;
Accepted manuscript posted February 1, 2016. doi:10.1115/1.4032652
Rolls-Royce plc

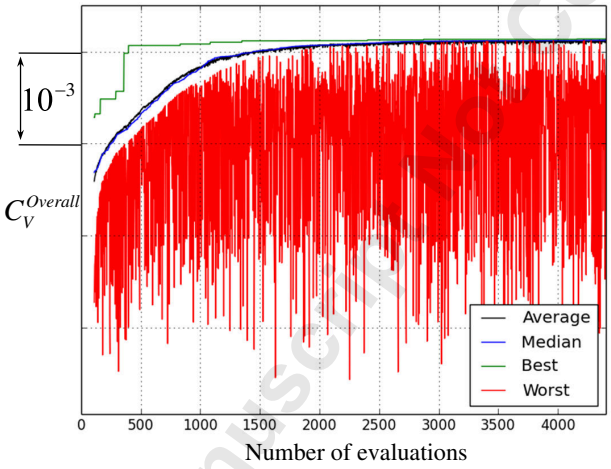

Fig. 11. Evolutionary computation for the optimization of $C_V^{Overall}$ – convergence process

Journal of Engineering for Gas Turbines and Power. Received November 22, 2015;
Accepted manuscript posted February 1, 2016. doi:10.1115/1.4032652
Rolls-Royce plc

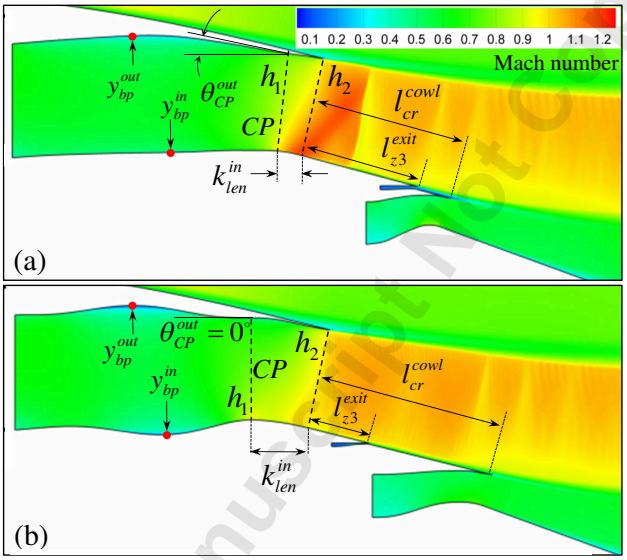

Fig. 12. Comparison between baseline and optimum exhaust designs for the future $E1$ engine architecture: (a) Baseline exhaust design, (b) Exhaust design optimized for $C_V^{Overall}$

Journal of Engineering for Gas Turbines and Power. Received November 22, 2015;
Accepted manuscript posted February 1, 2016. doi:10.1115/1.4032652
Rolls-Royce plc

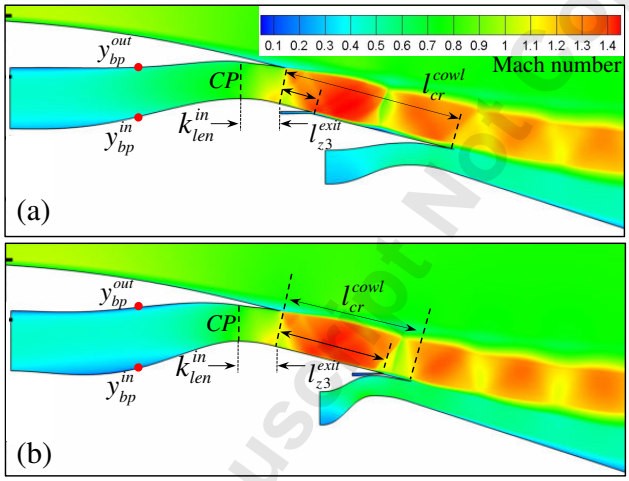

Fig. 13. Comparison between baseline and optimum exhaust designs for the current $E2$ engine architecture: (a) Baseline exhaust design, (b) Exhaust design optimized for $C_V^{Overall}$

2016-03-15

Aerodynamic design of separate-jet exhausts for future civil aero-engines, Part II: design space exploration, surrogate modeling, and optimization

Goulos, Ioannis

American Society of Mechanical Engineers

Goulos I, Otter J, Stankowski T, et al., (2016) Aerodynamic design of separate-jet exhausts for future civil aero-engines, Part II: design space exploration, surrogate modeling, and optimization. Journal of Engineering for Gas Turbines and Power, Volume 138, Issue 8, August 2016,Article number 081202. Paper number GTP-15-1539

https://doi.org/10.1115/1.4032652